100 year anniversary
Measurement Science and Technology

PAPER • OPEN ACCESS

Sizing of particles and droplets using 3D-PTV, an OpenPTV post-processing tool

To cite this article: R G Ramirez de la Torre and Atle Jensen 2023 *Meas. Sci. Technol.* **34** 065404

View the article online for updates and enhancements.

Sizing of particles and droplets using 3D-PTV, an OpenPTV post-processing tool

R G Ramirez de la Torre[1,2,*] and Atle Jensen[1]

[1] Department of Mathematics, Univeristy of Oslo, Oslo, Norway
[2] Faculty of Sciences, UNAM, Mexico City, Mexico

E-mail: reynar@math.uio.no and rgramtor@ciencias.unam.mx

Abstract

A methodology to obtain particle sizes from images was created, this tool can be used as a post-processing tool to the open source software OpenPTV. The proposed methodology uses the same images and information obtained during the 3D calibration of OpenPTV to estimate the real sizes of the observed particles. The objective of this paper is to introduce the followed methodology to create a sizing tool and validate the technique with different solid particles and water droplets. The method requires an extra calibration with a flat target containing circles of different sizes, but if the calibration is successful, the sizes of particles can be estimated reliably with a maximum relative error of 10%, as long as the particle diameter correspond to at least three pixels width in the obtained images.

Keywords: particle size, particle tracking, open source

(Some figures may appear in colour only in the online journal)

1. Introduction

In recent years, open-source software has become very popular in the scientific community. Open-source software has the advantage that the source code and interfaces are made available for the community to explore, modify and distribute. This facilitates the sharing of ideas, reduces costs and the time that is necessary to create new software. In addition, new features can be added and build upon a common platform, which facilitates the reuse of previous codes rather than individual in-house development, which is probably redundant throughout different research groups. In this work, a code

to obtain particle sizes was created. This code was designed to use together with the open source software OpenPTV [1]. OpenPTV is a collaborative effort of several research groups to develop a software for Particle Tracking Velocimetry in 3 Dimensions (3DPTV). The method consists in basically three steps: the identification of illuminated tracer particles from multiple camera views, a triangulation of the probable 3D location of the particles, and the link of particle locations in time to form probable particle trajectories. This technique is well-established and has been used to investigate 3D Lagrangian particle motion in turbulent flows [2–4]. To reconstruct particle trajectories, the accurate triangulation of the locations of tracer particles, and the unambiguous link of particles to form trajectories are needed. The goal of establishing such particle tracks is often to calculate Lagrangian velocities and accelerations. Today there exist different software with similar algorithms to perform PTV [5–7]. However, none of them present an extra feature where the sizes of the particles can be analysed simultaneously. Although, there are several studies that propose

---

* Author to whom any correspondence should be addressed.

techniques to measure sizes [8–10] and some of them, more recently have explored the possibility of having both features together [11, 12].

In some cases measurement of size of particles/droplets and kinematics of flow is important. This is needed to understand more complex phenomena and obtaining information of the flow in which the particles are immersed and its influence on the particles, see e.g. [13–16]. 3D particle tracking, and in particular OpenPTV, uses stereoscopic camera vision to achieve 3 dimensional tracing of the particles' positions. The triangulated location of the particles in 3D space was used to accurately estimate the size of the observed particles. In this way, for every time step in the image series, we can estimate the sizes of the imaged particles. The uncertainties in the positions of the particles depend primarily on the optical properties of the media involved, the imaging arrangement, the quality of the images and the quality of the calibration [17].

In the present work, a methodology to estimate the size of particles as an add-on to the tracking with OpenPTV is presented [18]. Optical sources of error were analysed to reduce the size estimation relative error. This analysis is presented in section 2.2. Furthermore, a validation of the methodology was made by comparing known sizes of solid particles and droplets. This validation can be found in section 3. The validation has been developed for ellipsoidal particles, as the goal is to study droplets. Future investigations can explore modifications for different shaped particles. This first attempt of the methodology has shown a maximum relative error of 10% . Further improvements can be made when considering other possible sources of error and other types of particles.

2. Methodology

The most common PTV setups include volumetric forward-scattering illumination by lasers, xenon lamps, LEDs or light projectors [8–10, 12, 19]. In this case, the most suitable illumination technique is backlighting using LED lights. By using backlighting we can obtain defined contours of the observed particles that can be translated into real size [20–22]. In addition, LED lamps are low cost and do not require a large number of safety rules as lasers do. On the other hand, there are a few disadvantages of LED-back-illumination. Nonetheless, with an appropriate optical setup, these effects can be minimised. For instance, LED lights may easily over-expose images. If there is no synchronization between the light and camera, fast-moving particles can result in blurry images due to long exposure times. This can be prevented by using a very fast shutter speed. The quality of the optical system can be determined by a series of equations [20, chapter 2], where we can establish the minimum measurable particle size ρ_m as:

$$\rho_m = \frac{2}{d_{\text{diff}}}, \quad d_{\text{diff}} = 2.44 f_{\#}(M+1)\lambda, \tag{1}$$

where $f_{\#}$ is the f-number of the lens, λ is the wavelength of the light source, and M is determined by the lens maker equation

as $M = z_0/Z_0$ with z_0 the distance to the image and Z_0 the distance to the focal plane. We can also establish the systems depth of field:

$$\delta_z = 2 f_{\#} d_{\text{diff}} \frac{M+1}{M^2}. \tag{2}$$

These equations can help us to to select the adequate parameters to assemble the experimental setup.

From images the pixel lengths for each particle in the vertical and horizontal axis, n_x and n_y, of the image can be retrieved. From this information we can calculate the diameter D_e or major and minor axis lengths l_x and l_y on x and y. Then, the pixel-to-world transformation, obtained in the calibration, will be applied to retrieve a length estimation along x and y. The accuracy of the length estimation will depend on the image resolution and quality, the accuracy of the particle tracking and how well we can defined the optical properties of the system. This depend mainly of the camera and lens characteristics and the illumination. In the following, a description of the proposed methodology will be conducted as a proof of concept for the development of such measurements.

2.1. Experimental setup

This study has been conducted in the Hydrodynamics Laboratory at the University of Oslo. The setup was situated in a wave tank with dimensions $25 \times 0.52 \times 1$ m. Figure 1 shows a schematic description of the setup. For the majority of this project, the tank has been kept water-free as the objective is to visualize water droplets moving through air. Four AOS Promon U1000 cameras were used and positioned on one side of the wave tank. The cameras had a resolution of 1920×1080 pixels and produced 8-bit gray scale images with a frame rate of 167 FPS. All four cameras captured a similar field of view (FOV). The illumination was provided by LED lamps on the opposite side of the tank and a white diffusive plastic sheet was used to distribute the light. According to equations (1) and (2), with the use of 50 mm lenses and $f_{\#} = 2$, this optical system is reliable to perform PIV or PTV for particles with diameters $D > 0.03$ mm in a volume of approximately 223 mm. Nonetheless, as we are interested on accurate size measurement, we required that the particles are larger than the pixel size (1 pixel = 0.2 mm), therefore, the analysed particles will have $D > 0.4$ mm.

To calibrate the PTV system, the method known as multiple plane calibration was used [23, 24]. This method consisted on taking images of a target in different planes of depth, i.e. moving the target in the z coordinate. The target consisted on a flat acrylic plate with an array of visible holes, evenly spaced every $10 \text{ mm} \pm 0.5 \text{ mm}$, as shown in figure 1(b). The positions of the holes in the target with reference to the coordinate system (x, y) were known. Then, the target was moved to 5 different depths: $z = -80, -40, 0, 40, 80$ mm (with a position error of 0.5 mm). With images of the different z, the epipolar geometry of the space can be defined [25]. After the calibration, the maximum error of the particle positions was up to 1.2 mm (close to the
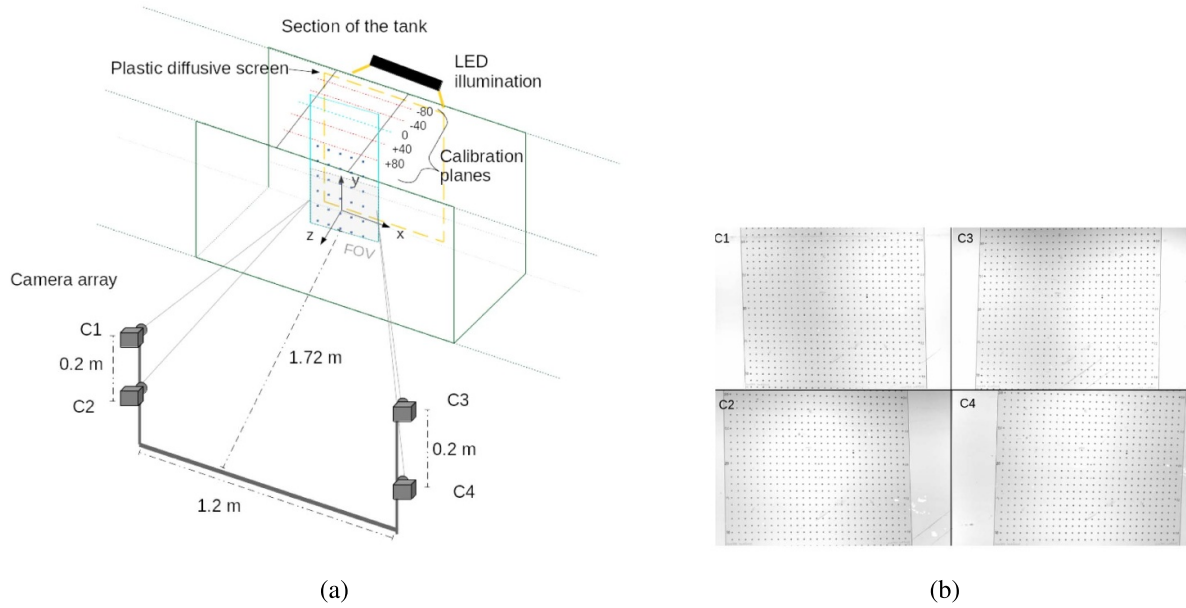
Figure 1. (a) Experimental setup where the PTV measurements are performed, the image shows the array of cameras positioned to visualise approximately the same field of view. The multiple planes for the calibration with a flat target are also depicted (b), together with the coordinate system orientation, with $z = 0$ in the centre of the tank, x parallel to the tank length and y in the vertical.

image edges) in the focal plane and up to 1.8 mm for out of focus depths. This corresponds to a relative error of less than 1% in the FOV.

PTV analysis typically (but not necessarily) uses images with a dark background and bright particles. However, this method produced images with a light background and dark particles, providing well-defined particle outlines. There are two options for analyzing images using OpenPTV software. One is to modify the code to detect bright particles on a dark background, which is feasible with open-source software. The other option is to invert the grayscale of the images to get bright particles on a dark background and then use these images directly in the code. While the first option may be more effective, it takes longer to precisely modify the code and requires careful development. Thus, for this project, the direct inversion of the images was used to align with the original code requirements. The result is that the PTV code analyzes images with bright particles on a dark background.

2.2. Determination of system parameters to estimate sizes in the analysis volume

For each particle p in the volume of observation, the goal was to obtain an estimate of the diameter $D^{(p)}$. From each camera C_i, the images gave a length in pixels for each axis: $n_{x,i}^{(p)}$ and $n_{y,i}^{(p)}$ for each visible particle in the images. This technique proposes to use a transformation:

$$T((x,y,z); n_{x,i}^{(p)}, n_{y,i}^{(p)}, \{C_i\}) = D^{(p)}, \qquad (3)$$

where (x, y, z) is the position of the particle p, as estimated by the OpenPTV software, and $\{C_i\}$ are other parameters determined by the optical system and can vary for each camera C_i in the setup. In this study, we detail the process of obtaining parameters and their application in this transformation. The camera parameters were established, and particle diameters were estimated using the transformation. The estimated particle diameters were then compared to previously measured values, allowing us to evaluate the accuracy of the method.

To estimate the necessary parameters for the sizing methodology and understand the limits of this technique, three parameter tests were done. The first test involved using images of the calibration target from the PTV calibration to determine the magnification change with respect to depth position. The results of this test are presented in section 2.2.1. The second and third tests consisted on using two different flat targets with circles and ellipses of different diameters from 0.3 mm to 50 mm. One of the targets contained only opaque figures (figure 3), while the second target contained figures with a gradient in their opacity (figure 4), simulating the characteristics of semi transparent particles. The targets were positioned in different depths, or z values, and OpenPTV was used to detect the positions of the circles and ellipses in the target. Then an estimation of their diameters was made and the effects of different intensities in the particle images were studied. The results of these tests are presented in section 2.2.2. To corroborate the precision of the found parameters for the transformation, the methodology was benchmarked against two different 3-dimensional arrays of solid particles and a group of droplets with different sizes distributed over the volume of observation.
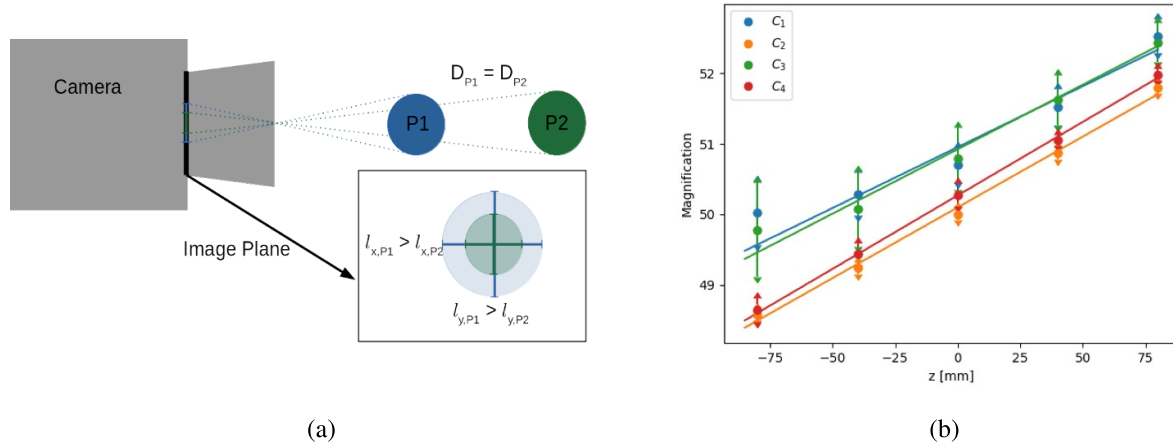
Figure 2. (a) A schematic description of the magnification in the image for two particles of the same diameter but with different z coordinate. (b): The linear magnification S_1 described in equation (4). The magnification changes with depth z, moreover, each camera C_i, $i \in [1, 2, 3, 4]$ in the array has its own linear fit.

The comparison of the results to the solid particles and the droplets will be shown in section 3.

2.2.1. Magnification dependency on system parameters.
The magnification, or ratio of pixels per centimetre in the image, varies depending on the distance between the imaged particle and the lens (figure 2(a)). For this camera setup, according to the pin-hole model, the magnification is expected to be linear. Nonetheless, each camera will have a different magnification which can be estimated. By using the calibration flat target with equidistant holes (described in section 2.1) and the different depth images of this target, the effects of the depth on the scale of the image were estimated. As the images of the target have different depth, or z coordinate, the pixel distance between the holes will vary while varying the position of the target along the z axis. Then, the magnification for each camera C_i was estimated as a function of z, see figure 2(b). This confirms that a linear fit approximate the magnification. However, each camera will have its own coefficients, which can be described as:

$$S_{1,i}(z) = \zeta_{1,i} z + \zeta_{0,i}. \tag{4}$$

In this way, $\zeta_{1,i}$ and $\zeta_{0,i}$ were calculated for each C_i. Then, the particle axis length in physical units, $l_{x,i}$ and $l_{y,i}$, for each C_i can be found as:

$$l_{x,i} = \frac{n_{x,i}}{S_{1,i}(z)}, \quad l_{y,i} = \frac{n_{y,i}}{S_{1,i}(z)}, \tag{5}$$

where $n_{x,i}, n_{y,i}$ are the number of pixels in the axis, x and y respectively, of the particle seen in each camera i. If the image of the particle is assumed to be elliptical, we use the unique length measurement to identify particles sizes denominated as equivalent diameter, defined as $D_e = \sqrt{l_x l_y}$, where l_x and l_y are the axis lengths of the particle in x and y approximated as an ellipse in each image. Using the definition of D_e, the equivalent

diameter of some particle p from a particular camera C_i can be described as:

$$D_i^{(p)} = \sqrt{\frac{n_{x,i}}{S_{1,i}(z)} \frac{n_{y,i}}{S_{1,i}(z)}} = \frac{\sqrt{n_{x,i} n_{y,i}}}{S_{1,i}(z)}. \tag{6}$$

Then, an average D_e can be obtained by considering all the values determined for each camera i:

$$D_e^{(p)} = \overline{D_i^{(p)}} = \frac{1}{4} \sum_{i=1}^{4} D_i^{(p)}. \tag{7}$$

This average will be interpreted as the diameter of the particle.

2.2.2. Relative intensity as a system parameter.
The particles are defined in the PTV algorithm by the detection of blobs or edges in the image together with a threshold in the grey level or intensity. This value between 0 and 255 has been fixed by the user during the image processing. The threshold value varies in each experiment due to factors such as camera setup, lighting, and particles being observed. It's crucial to establish a generalised approach to estimate the impact of the threshold on measurements. One approach is to use relative intensity, which compares the user-defined threshold to the maximum intensity in the images. The following describes the procedure used to consider relative intensity in this methodology.

The particles are distinguished by pixel area and pixel length in the vertical and horizontal direction. These lengths and area are defined by the intensity threshold, which therefore has a direct impact in the approximated size of the particle. By using the test targets (figures 3 and 4), the equivalent diameter for the different sizes, shapes and intensities were obtained and compared with the measured diameters by calculating the ratio D_e/D_r, where D_e comes from the estimation in equation (7) and D_r is the measured diameter. This ratio showed values as high as 2.3, which means some diameters are overestimated by more than 100%. The difference in intensity for each
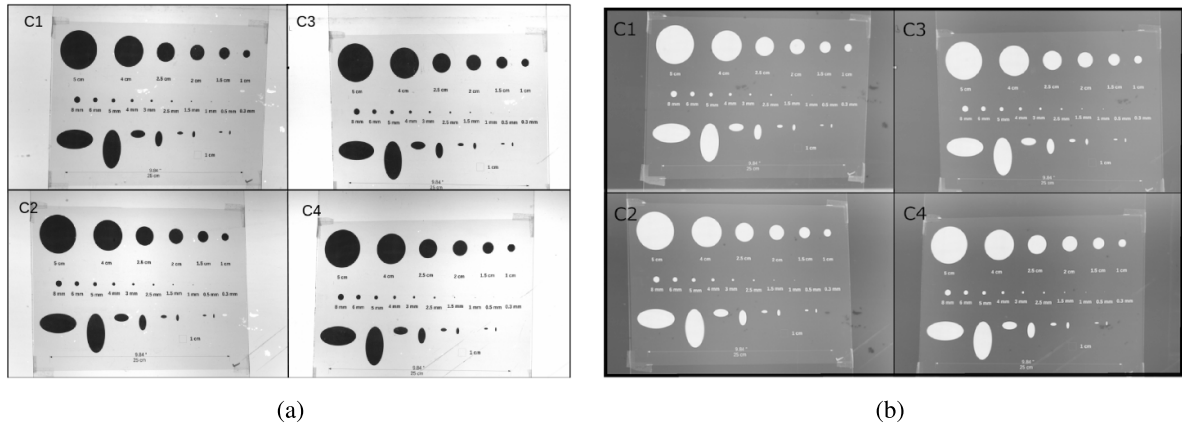
Figure 3. Example of images from the flat target with dark circles taken with the camera array; the original images (a), and the inverted images used for PTV and sizing methodology (b).
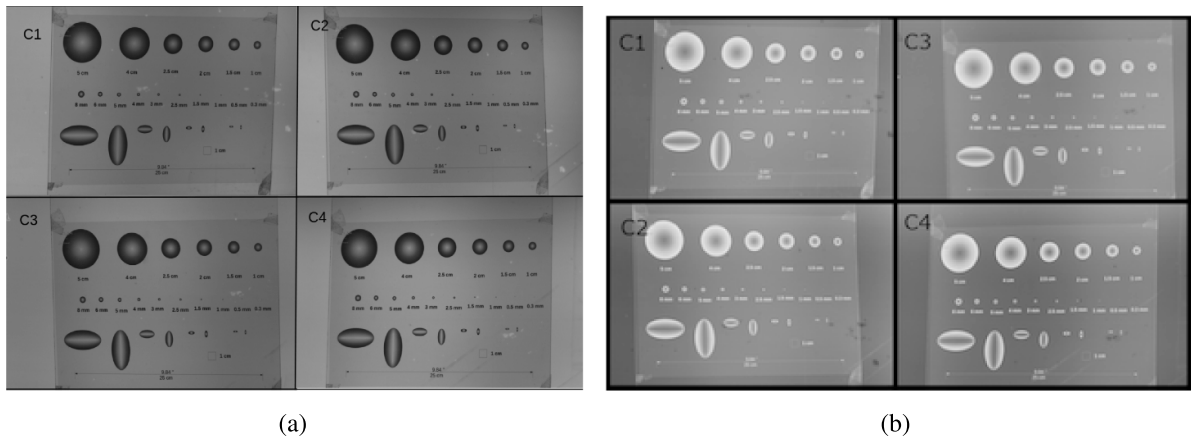
Figure 4. Example of images from the flat target with gradient opacity circles taken with the camera array: the original images (a), the inverted images used for PTV and sizing methodology (b).

particle showed a correlation to the overestimation of the diameter.

Depending on the optical arrangement and the light scattering, the inverted images will have a maximum intensity I_{max} (in the original images, it is the intensity minimum), that varies with each set of images and type of particles. For this particular setup, in the targets presented in figures 3 and 4, the completely opaque circles have $I_{max} = 70$, while the circles with an opacity gradient have $I_{max} = 50$. To quantify the importance of the intensity changes we can refer to figure 5. This figure shows the empirically found relation between the relative intensity I/I_{max} and the ratio D_e/D_r for the test targets. We see this is a non-linear relation with a peak that corresponds to particles with a diameter around 24 pixels. It is reasonable to assume that the peak at 24 pixels is due to errors from the particle illumination pattern and pixel size. While lower intensity decreases error for larger particles, with particle diameters around 24 pixels, high intensity exacerbates the error caused by pixel size. This effect should be investigated further and understanding of its pixel value in relation to the optical system should be obtained. For the purpose of this investigation, it is enough to study the effect for this particular setup.

From the found relation, two cases were defined to simplify the approximation as polynomials; particles with imaged diameter below 24 pixels and particles with diameter equal or above 24 pixels. In the case of particles with imaged diameter $d^{(p)} < 24$, the pixel size of the particles becomes the largest source of error and it also increases with the intensity of the particle. On the other hand, particles with imaged diameter $d^{(p)} \geqslant 24$ outside of the focal plane will have a larger Gaussian filter size and therefore more blurry image with a diameter $d^{(p)}$ larger than a particle with same D_r in the focal plane (figure 5). It will also have an intensity per pixel I_p smaller than the value for the particle close to the focal plane, therefore the value $D_e^{(p)}$ will be larger than the value obtained for a focused particle of the same D_r. In both cases, the ratio of the estimation to the measured size $S_2 = \frac{D_e}{D_r}$ was plotted against the relative intensity per pixel $I = \frac{I_p}{I_{max}}$ of the detected particles, as shown in figure 5, the correlations were approximated by second order polynomials:

$$S_2(I, d) = \alpha_2(d)I^2 + \alpha_1(d)I + \alpha_0(d), \qquad (8)$$

where $d = \sqrt{\overline{n_{x,i}}, \overline{n_{y,i}}}$, and the coefficients α depend on d as defined previously for cases when $d < 24$ pixels and $d \geqslant 24$

(a)   (b)
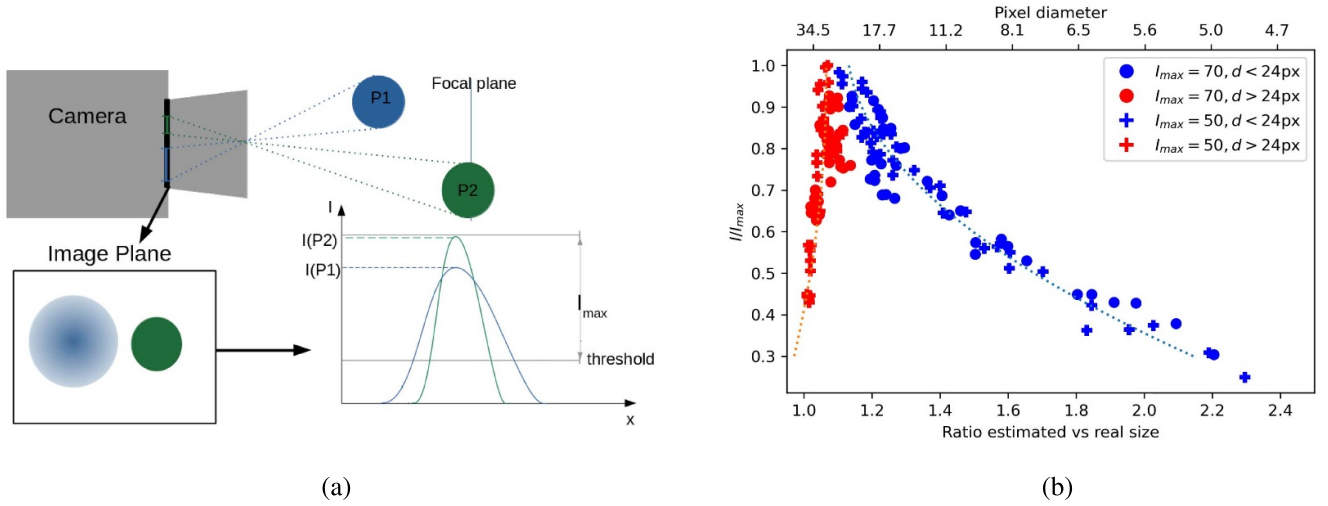
Figure 5. (a) Schematic representation on how the intensity and depth are related to the change in imaged size. For a particle in the focal plane the estimated diameter is smaller and the intensity is larger than a particle out of focus. (b) The graph shows the ratio between the estimated size and the real size compared to the relative intensity per pixel. The different circle arrays are distinguished by symbol: ● for array with opaque circles, + for array with opacity gradient. The colour distinguish the particle size, red for particles with $d \geqslant 24$ pixels, the maxima of the data, and blue for particles with $d < 24$ pixels. The solid lines show the fit corresponding to equation (8) for the relative intensity per pixel for the different arrays of circles. These polynomials will be used to correct the estimation for particles with low contrast depending on their size.

(a)   (b)
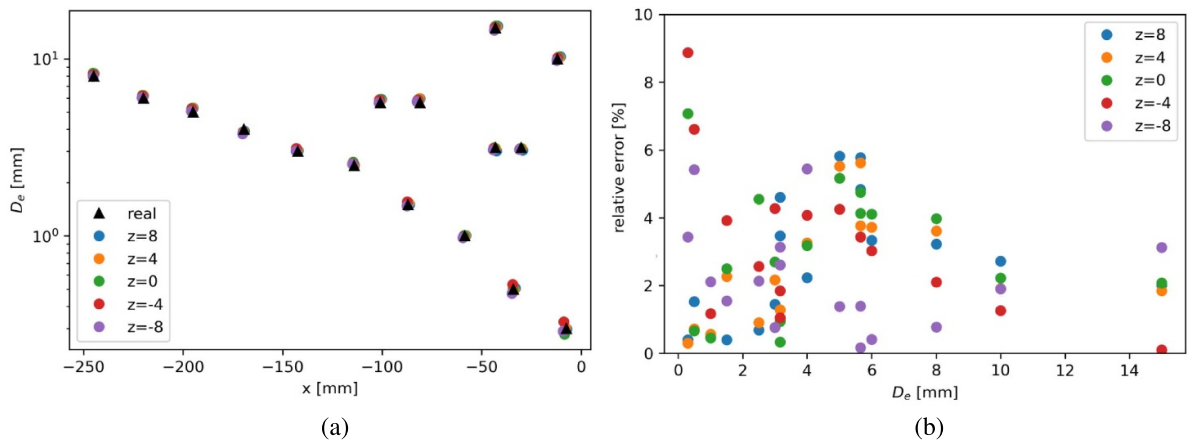
Figure 6. Results of the proposed size estimation applying the transformation $T(z; n_{x,i}, n_{y,i}, I)$. (a) The estimated size compared to the real size of the different circles and ellipses in the target at different depths (z coordinate); (b) the relative error of this estimation compared to the real size.

pixels. Then, the equivalent diameter of each particle can be estimated as:

$$D_{e,i} = \frac{\sqrt{n_{x,i} n_{y,i}}}{S_{1,i}(z) S_2(I, d)}. \qquad (9)$$

With this equation we have obtain an estimation of the equivalent diameter of a particle for each camera where the particles is visible. To make a single estimate per particle, an average can be used so that the final approximation is:

$$D_e = \frac{1}{N} \sum_{i=1}^{N} D_{e,i} = T(z; n_{x,i}, n_{y,i}, I), \qquad (10)$$

where N is the total number of cameras used. This is the transformation T, as proposed in equation (3) where the most relevant parameters were shown to be the depth of the particle and its mean intensity per pixel. In figure 6 we show the result by using the proposed transformation to the test targets which gives relative errors: $\frac{|D_r - D_e|}{D_r} \times 100 \leqslant 10\%$.

3. Validation on solid particles and water droplets

After obtaining the transformation, the procedure was validated in 3-dimensional arrays with different types of particles and with water droplets. The first particle array (**G1**) consisted of solid fishing lead weights of three different sizes; images of **G1** can be seen in figure 7. The dimensions of the particles

(a)   (b)
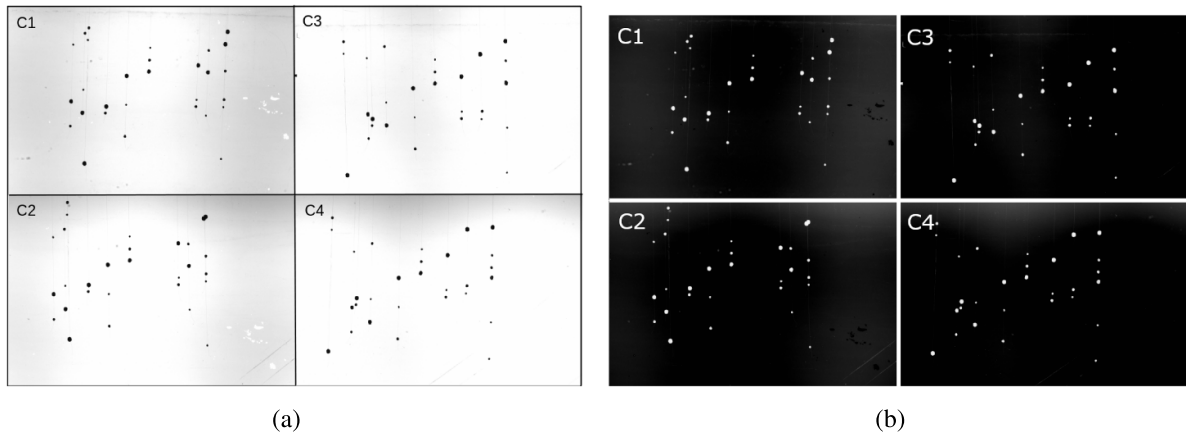
Figure 7. Original images (a) and inverted images (b) for the array with 30 particles (**G1**), with 3 sets of 10 particles with different sizes: 2.5, 3.5, 5.5 mm with measurement error of 5%.

(a)   (b)
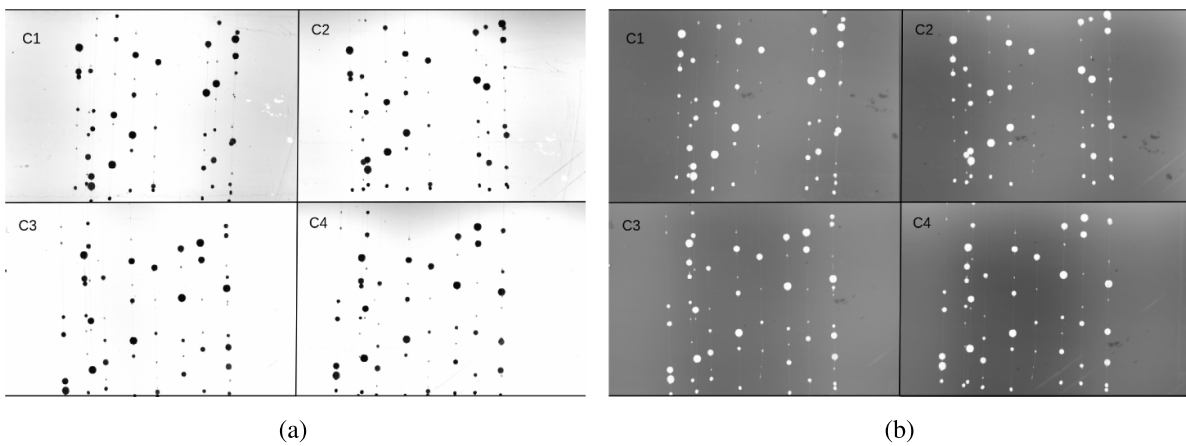
Figure 8. Original images (a) and inverted images (b) for the array with 57 particles (**G2**), with 6 sets of 10(or 7) particles with different sizes: 9.5, 7.8, 5.8, 4.2, 2.1 and 1.5 mm with a measurement error of 2%.

were manually measured to make an equivalent diameter value for each particle size. The particle sizes are approximately 2.5, 3.5 and 5.5 mm, with a measurement error of 5% in all cases. The comparison between the real sizes and the estimated sizes is presented in figure 9, the maximum relative error is below 6%. The other three-dimensional array (**G2**) was made with plastic beads, some of them transparent and others opaque. In total, 57 particles of 6 different sizes were distributed in the volume. This array is presented in figure 8. The six different sizes are 9.5, 7.8, 5.8, 4.2, 2.1 and 1.5 mm with a measurement error of 2%. The proposed sizing estimation was applied to **G2**, and the results are also presented in figure 9.

In figure 9(b), the particles in **G2** which are translucent are marked by the dotted ellipse. It is evident that the error in this cases is larger than 10%. However, the error increases for only these cases in all the samples considered. The reason why this happens is very simple; **G2** is the only set where particles of different opacity were analysed. The relative intensity relation found by S_2 (equation (8)) is affected by I_{max} of the opaque particles in **G2**, and therefore an overestimation will be done for the translucent particles. This can be explained with an

example. Consider two particles p_1 and p_2 with the same size but different opacity and $d < 24$ pixels. Let us also assume that the opacity of p_2 is larger than the opacity of p_1. For their intensities per pixel, it will be valid that $I_p(p_1) < I_p(p_2)$, due to the different opacity, and accordingly their relative intensity $I(p_1) < I(p_2)$. According to equation (9), the correction for intensity is inversely proportional to the intensity, therefore $D_e(p_1) > D_e(p_2)$ a larger correction will be made for particle p_1. Which in this case will lead to an overestimation of the size. Because of this, it is recommended that the proposed methodology should be used only when the analysed particles have similar opacity, for example, analyse only drops of the same liquid, or liquids with similar light absorption properties.

Finally, the methodology was validated with falling water droplets. Droplets of different sizes were generated using different flat-edged needles with distinct diameters. At a constant flow rate, each needle releases droplets of the same size from the tip, where the droplet diameter is proportional to the needle diameter. The droplets fall freely to be recorded in a short time interval. The droplet size can be approximated by weighting each of the released droplets. As the droplets are composed of

<center>(a)</center> <center>(b)</center>
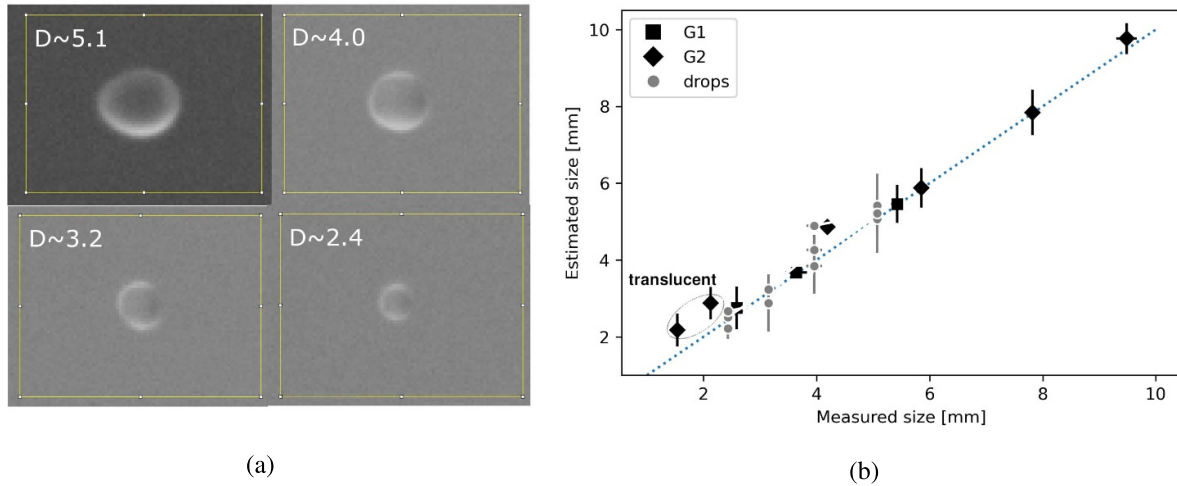
Figure 9. (a) Example of images of droplets in the different sizes. The yellow line delimits an area of 60 by 80 pixels. (b) Comparison between measured sizes and estimated sizes by the proposed methodology for the different particle arrays and the falling droplets. **G1** refers to the array with 30 lead weights and **G2** refers to the array with glass beads. Error bars are shown for both the measurements and the estimations. The dotted line shows the identity line, where the measured size is equal to the estimation.
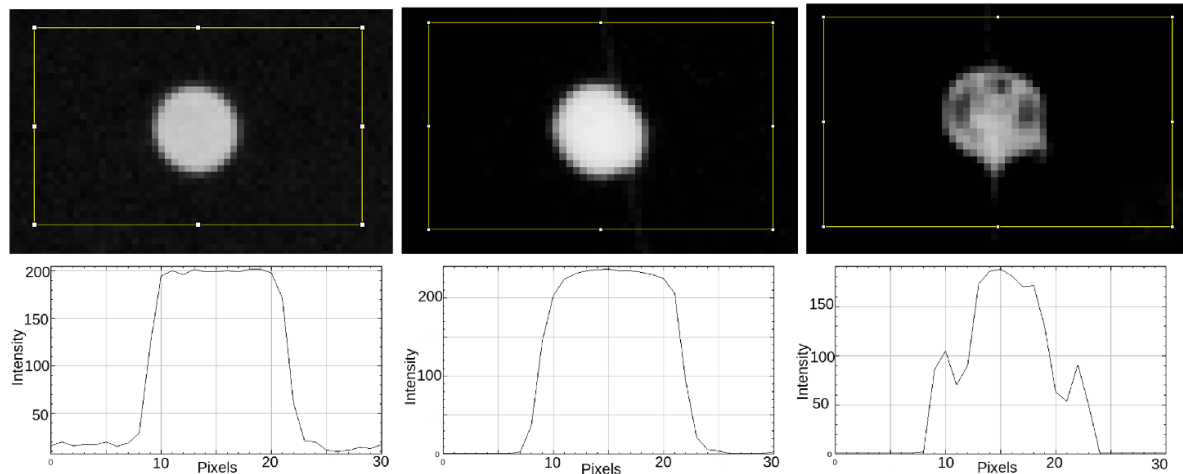
Figure 10. Comparison between different cases of a particle with diameter close to 2.5 mm. The yellow line delimits an area of 30 by 50 pixels. The intensity plots corresponds to each case above and they show the gray value per pixel in the centre line of the particle, which is equivalent to the pixel length of the particle in the horizontal direction. From left to right: a circle from flat target, a particle from **G1** and a particle from **G2**. It is visible that the translucent particle (right) will have in average lower intensity per pixel than solid particles.

clean water at $20\,^{\circ}$C, the diameter of a spherical droplet can be obtained by the equation:

$$D = \sqrt[3]{\frac{3m}{4\pi\rho}}, \qquad (11)$$

where m is the measured mass of the droplet and ρ is the density of water at $20\,^{\circ}$C. Images of the different droplets were taken with the same system, some of the obtained images are shown in figure 9. Four different sizes of droplets were achieved with diameters between 2.4 and 5.1 mm with a measurement error of 3%. The proposed methodology was applied to the time series of the falling droplets and the results are presented in figure 9. We see that using the same methodology,

we can approximate the droplet sizes within the estimation error. It is worth mentioning that the results for the falling droplets show that the methodology works also for moving particles.

As discussed earlier, when obtaining the transformation in equation (9), the assumption that all the visible particles have similar response to the light was implicit. Therefore, introducing translucent particles together with opaque particles affected the accuracy of the method for the translucent particles, as shown in the results for **G2**. In figure 10, the different intensity profiles for some of the used examples in the validation are presented. It is visible that the translucent particle has a more variable intensity profile and a smaller $I_{\max}$. The intensity per pixel I_p will be smaller and

if compared to the maximum intensity of another particle, their relative intensity will be smaller than it should be when compared to their own I_{max}. That is what happened in the array **G2**. Nonetheless, if the particles' response to the light is similar for all, the estimation will be accurate as seen for **G1** and the water droplets. Moreover, if the optical characteristics of the particles to analyse are known, the parameters for the transformation can be proposed in a way that it will account for these. The main source of error will be the parameters that has not been predicted during the transformation's acquisition.

4. Concluding remarks

In this study, a method for determining particle sizes was introduced. This tool is intended to be utilized as a post-processing addition to the open-source software OpenPTV. The methodology was based on analysing possible sources of error in the optical system and estimation of sizes from the information already obtained by OpenPTV. The proposed methodology required an extra calibration, where the image intensity, the relative intensity of the particles, the position of the particles and the particle pixel size can be correlated to give a size estimate. Then the tool was validated by comparing the known sizes of different particles to the estimation obtained by the proposed tool.

Three different types of particles were used in the validation; opaque solid particles, translucent solid particles and water droplets. This has been a first attempt on estimating sizes from the PTV information, which proved to give relative errors of the estimation below 10%. The investigated particles were mostly spherical or ellipsoidal, but the methodology can be modified in order to consider other shapes. For example, by considering pixel area instead of diameter in each direction and calculating particle volume. The volume or elongation in the depth direction is estimated by the stereo position of the cameras, giving reliable measurements even for elongated particles. However, further studies should be made to analyse the sources of error for that case. Another limitation of the presented methodology is that only particles of similar opacity can be analysed in the same time series. As the maximum intensity is an important parameter in the equation to estimate sizes (equation (9)). This means only particles of the same material or at least similar optical properties can be analysed by this methodology.

Finally, it is important to notice, that the methodology can be used for time series of unblurred images of moving particles, e.g. falling droplets. If these requirements are met, the size estimates will remain accurate with no change in error. With this methodology it is possible to perform meaningful size analysis of 3D moving particle systems. Size distribution has been found in studies of droplet formation by breaking waves, see [26]. The results showed that the droplet size distribution estimated with this method was similar to those found by other studies. In the future other sources of error in the methodology can be explored to give a more robust estimation of the overall error.

ORCID iD

R G Ramirez de la Torre ⬤ https://orcid.org/0000-0002-2447-5946

References

[1] OpenPTV Consotium 2014 OpenPTV. Open source particle tracking velocimetry (available at: www.openptv.net)
[2] Maas H G, Gruen A and Papantoniou D 1993 Particle tracking velocimetry in three-dimensional flows *Exp. Fluids* **15** 133–46
[3] Malik N A, Dracos T and Papantoniou D A 1993 Particle tracking velocimetry in three-dimensional flows *Exp. Fluids* **15** 279–94
[4] LÜTHI B, Tsinober A and Kinzelbach W 2005 Lagrangian measurement of vorticity dynamics in turbulent flow *J. Fluid Mech.* **528** 87–118
[5] Schanz D, Schröder A, Gesemann S, Michaelis D and Wieneke B 2013 Shake the box: a highly efficient and accurate tomographic particle tracking velocimetry (TOMO-PTV) method using prediction of particle positions *10th Int. Symp. on Particle Image Velocimetry* (*Delft, Netherlands, 2013*) pp 1–13
[6] Tan S, Salibindla A, Masuk A U M and Ni R 2020 Introducing openlpt: new method of removing ghost particles and high-concentration particle shadow tracking *Exp. Fluids* **61** 1–16
[7] Shnapp R 2022 MyPTV: a python package for 3d particle tracking *J. Open Source Softw.* **7** 4398
[8] Bachalo W D and Houser M J 1984 Phase/Doppler spray analyzer for simultaneous measurements of drop size and velocity distributions *Opt. Eng.* **23** 235583
[9] Lee Black D, Queiroz McQuay M and Bonin M P 1996 Laser-based techniques for particle-size measurement: a review of sizing methods and their industrial applications *Prog. Energy Combust. Sci.* **22** 267–306
[10] Nobach H, Damaschke N and Tropea C 2002 Optical limits of particle concentration for multi-dimensional particle sizing techniques in fluid mechanics *Exp. Fluids* **32** 143–52
[11] Masuk A U M, Salibindla A and Ni R 2019 A robust virtual-camera 3d shape reconstruction of deforming bubbles/droplets with additional physical constraints *Int. J. Multiph. Flow* **120** 103088
[12] Koothur V 2021 Tracking and sizing of particles in the Mie scattering regime using a laser scanning technique *PhD Thesis* Norwegian University of Science and Technology

[13] Dehghani S R, Naterer G F and Muzychka Y S 2016 Droplet size and velocity distributions of wave-impact sea spray over a marine vessel *Cold Reg. Sci. Technol.* **132** 60–67

[14] Deike L 2022 Mass transfer at the ocean–atmosphere interface: the role of wave breaking, droplets and bubbles *Annu. Rev. Fluid Mech.* **54** 191–224

[15] Mueller J A and Veron F 2009 A sea state–dependent spume generation function *J. Phys. Oceanogr.* **39** 2363–72

[16] Veron F 2015 Ocean spray *Annu. Rev. Fluid Mech.* **47** 507–38

[17] Dracos T 1996 Particle tracking in three-dimensional space *Three-Dimensional Velocity and Vorticity Measuring and Image Analysis Techniques* (Berlin: Springer) pp 209–27

[18] Ramirez de la Torre R G 2022 particle_sizing (Zenodo) (https://doi.org/10.5281/zenodo.6953983)

[19] Katz J and Sheng J 2010 Applications of holography in fluid mechanics and particle dynamics *Annu. Rev. Fluid Mech.* **42** 531–55

[20] Raffel M, Willert C E and Kompenhans J *et al* 1998 *Particle Image Velocimetry: a Practical Guide* vol 2 (Berlin: Springer)

[21] Hagsäter S M, Westergaard C H, Bruus H and Kutter J P 2008 Investigations on led illumination for micro-piv including a novel front-lit configuration *Exp. Fluids* **44** 211–9

[22] Bröder D and Sommerfeld M 2007 Planar shadow image velocimetry for the analysis of the hydrodynamics in bubbly flows *Meas. Sci. Technol.* **18** 2513

[23] Castello L D 2007 Multi-plane calibration (available at: https://openptv-python.readthedocs.io/en/latest/add_doc.html)

[24] Goumnerov H 2007 Openptv. installation and user manual (available at: https://openptv-python.readthedocs.io/en/latest/add_doc.html)

[25] Maas H-G 1996 Contributions of digital photogrammetry to 3-d PTV *Three-Dimensional Velocity and Vorticity Measuring and Image Analysis Techniques* (Berlin: Springer) pp 191–207

[26] Ramirez de la Torre R G, Vollestad P and Jensen A 2022 Experimental investigation of droplet generation by post-breaking plunger waves *Water Waves* **4** 1–21